http://dx.doi.org/10.14500/aro.12716

Modeling the Influence of Nitrogen Concentration on Optical Gain Performance in Gallium Nitride Arsenide/Gallium Arsenide Quantum Wells Vertical-cavity Surface-emitting Lasers

Amanj L. Shafiq†, Faten A. Chaqmaqchee, and Mohammad Gh. Faraj

Department of Physics, Faculty of Science and Health, Koya University,
Koya 44023, Kurdistan Region – F.R. Iraq

***Abstract*—This study investigates the influence of nitrogen (N) concentration on the optical and gain characteristics of Gallium Arsenide (GaAs)/gallium arsenide (GaAs) quantum wells (QWs) based vertical-cavity surface-emitting lasers (VCSELs) using MATLAB simulations. Numerical simulations were performed how varying N content affects cavity design and optical confinement properties. The stopband behavior and resonant wavelength shift were analyzed through reflectivity spectra for different N concentrations. The results reveal a red shift in the resonance wavelength and redistribution of the electric field intensity within the cavity as the N concentration increases. Higher N concentrations reduce mirror losses. However, excessive N incorporation introduces scattering and interface imperfections, leading to increased internal losses. In addition, an increase in N percentage results in reduced optical confinement factor and material gain decrease, indicating a lower overlap between the optical field and the active area. Both the threshold density and transparency carrier density were observed to rise with N addition, implying a decrease in recombination performance. Reflection-mode spectra confirm a red shift and a reduction in gain peak with higher N content. This analysis focused on a critical design of GaNAs VCSEL structure, which makes a distinction between engineering index profiles for optimal gain overlap and adjusting the optical path length for spectral control. A N concentration in the range of 1–2% provides the optimal balance along gain enhancement, optical confinement, loss minimization, and reflection gain, which are (0.11, 0.099), (175 cm^{-1}, 162 cm^{-1}), and (20.26 dB, 19.66 dB), respectively, thereby providing the overall performance of GaNAs/GaAs QWsVCSELs.**

***Index Terms*—Distributed Bragg reflectors, Gallium nitride arsenide/gallium arsenide, Nitrogen concentration, Optical gain, Vertical-cavity surface-emitting lasers.**

ARO-The Scientific Journal of Koya University
Vol. XIV, No.1 (2026), Article ID: ARO.12716. 201 pages
DOI: 10.14500/aro.12716
Received: 02 November 2025; Accepted: 19 February 2026
Regular research paper; Published: 14 April 2026
†Corresponding author's e-mail: amanj.lateef@koyauniversity.org

I. Introduction

Vertical-cavity surface-emitting lasers (VCSELs) have achieved significant progress over the past decades, making them a suitable choice over the conventional edge-emitting lasers (Cao, 2020, Wu et al., 2024). Their low cost, low divergence, circular shape, and high efficiency make them highly attractive for various photonic applications, including optoelectronic, semiconductor lasers, and optical detectors (Xu, Cheng, and Huang, 2009, Li et al., 2015, Liu et al., 2019, Tian, Ahamed, and Bimberg, 2023, Yu et al., 2023, Jaffal et al., 2024, Chaqmaqchee, 2024, Gilli, Cossu, and Ciaramella, 2025, Wang et al., 2025). Enhancing a well-designed VCSEL is essential for optimizing its performance across a wide spectrum, from short to long wavelengths range (Alexandre et al., 2002, Ebeling, Michalzik, and Moench, 2018, Chaqmaqchee et al., 2020, Abdullah and Chaqmaqchee, 2025), enabling them to be suitable for diverse fields such as laser printing (Liu et al., 2019), fiber-optic communication (Hai et al., 2000, Wang et al., 2025), and gas sensing (Yu et al., 2023). In VCSELs, QWs incorporate dilute nitrides, where small amounts of nitrogen (N) are introduced into III-V compounds semiconductors. This modification imparts remarkable electrical and optical properties (Pozina et al., 1998, Takeuchi et al., 1998, Hestroffer et al., 2018, Guina, Wang, and Aho, 2018). Among the most significant dilute nitrides are Gallium Arsenide (GaAs) (Takeuchi et al., 1998, Alexandre et al., 2002, Babichev et al., 2023), GaInNAs (Onishi et al., 2009, Chaqmaqchee, 2020) and GaInNAsSb (Chaqmaqchee, 2016, Chakir et al., 2017, Chaqmaqchee et al., 2020). By substituting a small proportion of the group V atoms with N, these materials exhibit unique characteristics due to their distinct size and electronegativity. This enables significant progress in long-wavelength optoelectronic devices (Takeuchi et al., 1998, Guina, Wang, and Aho, 2018) while also reducing the lattice constant (Guina, Wang and Aho, 2018). A VCSEL operates either electrically or optically, injecting electrons and holes in the active area (Zhang et al., 2007, Liu et al., 2019). The reduced bandgap of the quantum wells (QWs) helps concentrate carriers (Moatlhodi, Ditshego

and Samikannu, 2020). Various dilute nitride materials have been used as QWs in different studies to achieve higher gain in reflection mode demonstrating their ability to propagate emission wavelengths into the long wavelength region (Lisesivdin et al., 2014, Chaqmaqchee et al., 2020, Chaqmaqchee, 2020, Yaba and Chaqmaqchee, 2022).

Distributed Bragg reflectors (DBRs) are widely used in optical devices to achieve high reflectivity over a narrow wavelength range, enabling efficient optical confinement and minimal propagation loss (Swara, Chaqmaqchee, and Sediq, 2025, Watanabe et al., 2025). For our structure, aluminum arsenide (AlAs)/gallium arsenide (GaAs) were selected because they offer high reflectivity with fewer mirror pairs due to their large refractive index contrast and excellent lattice compatibility. This materials combination lowers strains, reduces defect formation during growth (Onishi et al., 2009, Muszalski, Sankowska, and Kucharski, 2020). In addition, AlAs and GaAs can be combined with AlGaAs as spacer layers adjacent to the GaNAs/GaAs active region, enabling continuous epitaxial growth. Notably, the AlAs/GaAs stack becomes optically transparent at the operating wavelength when using the selected N concentration in the QWs GaNAs, making it the most suitable mirror system for the designed VCSEL.

To further highlight the novelty of this work, we have added a comparison of previously reported dilute nitride materials with our study, focusing on their key properties for long-wavelength VCSELs. Various dilute nitride materials have been used as QWs in different studies to achieve higher reflection gain and to extend emission wavelengths into the long-wavelength region. Table I summarizes the materials, DBR configurations, device types, target wavelengths, and reflection gains reported in the literature, alongside the results of the present work.

As shown, while previous studies mainly focused on vertical-cavity semiconductor optical amplifiers and specific compositions of InGaAsN or GaInNAsSb QWs for wavelengths around 1288–1300 nm, the present study provides a systematic analysis of GaNAs/GaAs QWs in VCSELs over a range of N concentrations (0.4–3%). This enables a detailed investigation of the influence of N concentration on optical performance metrics such as reflection gain and emission wavelength. Our results demonstrate both the achievable wavelength tuning and the corresponding gain values, offering new insights for the design of long-wavelength VCSELs with dilute nitride QWs.

To expand the range of materials available for long-wavelength VCSELs and enhance the optical gain, we designed and implemented the GaNAs QWs with varying N concentrations, a material system not previously employed as QWs in VCSELs structures. GaN_xAs_{1-x} offer several advantageous properties that make it a strong candidate for long wavelength operation. First, GaNAs exhibits a large bandgap bowing parameter, enabling significant bandgap reduction with only a small incorporation of N. In addition, it maintains nearly lattice-matched growth on GaAs substrate, allowing efficient emission at longer wavelengths. By introducing N concentration of x = 0.4%, 1.2%, 2%, and 3% into the GaAs layer to form GaN_xAs_{1-x}, the bandgap energy decreases correspondingly to approximately 1.3 eV, 1.18 eV, 1.105 eV and 1.05 eV, respectively (Buyanova et al., 2001, Sanna and Fiorentini, 2004, Takao et al., 2006, Fujii et al., 2007, Goshima et al., 2011, Balakrishnan et al., 2014, Gelczuk et al., 2016, Sun et al., 2018, Jansson et al., 2024). Second, photoluminescence studies have shown that GaNAs exhibits stable and well- defined optical transitions across a range of N concentrations, demonstrating suitability for high-performance optoelectronic devices (Buyanova et al., 2001, Takao et al., 2006, Sun et al., 2018). Moreover, the precise controllability of N concentration provides a tunable emission wavelength, making it attractive for telecom-wavelength operations. Taking together, these characteristics collectively make GaN_xAs_{1-x}/GaAs a promising active region material system for longer-wavelength VCSELs. The present study addresses this gap by investigating the use of GaNAs as the QWs materials in VCSEL structures.

II. Materials And Methods

The VCSEL structure is generally formed by positioning an active region and spacer layers between two highly reflective cavity mirrors (Liu et al., 2019, Yu et al., 2023). Fig. 1 illustrates the schematic structure cross-section of the top-emitting VCSEL design, which comprises GaNAs/GaAs MQWs sandwiched between AlGaAs spacer layers, and enclosed by the AlAs/GaAs DBRs on both the top and bottom sides. In the simulated VCSEL structure, all layers are assumed to be formed on a GaAs substrate to represent

TABLE I
A Comparison of Dilute Nitride Materials and Their Key Properties for Long-Wavelength Vcsels

QW material	DBR pairs	Devices	Targeted wavelength (nm)	Reflection gain (dB)	References
$In_{0.35}Ga_{0.65}As_{0.975}N_{0.025}$	AlGaAs/GaAs	VCSOA	1288.5	20	(Lisesivdin et al., 2014)
$Ga_{0.61}In_{0.39}N_{0.0033}As_{0.9876}Sb_{0.016}$	AlGaAs/GaAs	VCSOA	1300	53.2	(Chaqmaqchee et al., 2020)
$Ga_{0.65}In_{0.35}N_{0.02}As_{0.98}$	AlGaAs/GaAs	VCSEL	1300	21	(Chaqmaqchee, 2020)
$Ga_{0.7}In_{0.3}N_{0.038}As_{0.962}$	AlGaAs/GaAs	VCSOA	1300	36	(Yaba and Chaqmaqchee, 2022)
$GaN_{0.004}As_{0.996}$	AlAs/GaAs	VCSEL	954	24	This work
$GaN_{0.012}As_{0.988}$	AlAs/GaAs	VCSEL	1050	20.26	This work
$GaN_{0.02}As_{0.98}$	AlAs/GaAs	VCSEL	1122	19.66	This work
$GaN_{0.03}As_{0.97}$	AlAs/GaAs	VCSEL	1181	10	This work

AlAs: Aluminum arsenide, GaAs: Gallium arsenide, Aluminum gallium arsenide, DBR: Distributed Bragg reflectors, QWs: Quantum wells, VCSELs: Vertical-cavity surface-emitting lasers, VCSOAs: Vertical-cavity semiconductor optical amplifiers

 http://dx.doi.org/10.14500/aro.12716

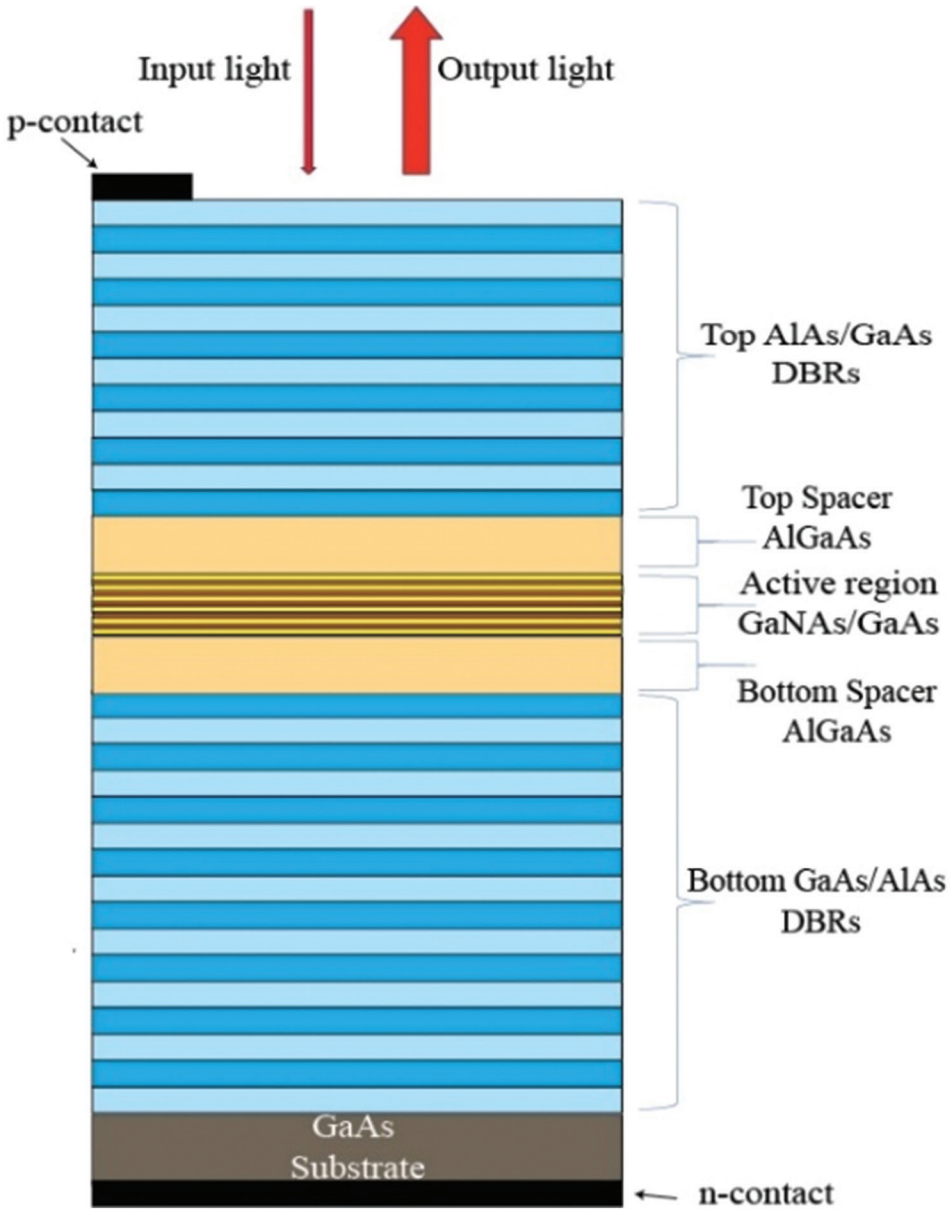

Fig. 1. Schematic diagram of the vertical-cavity surface-emitting laser structure showing the distributed Bragg reflectors, active region, and optical emission pathway.

the actual device configuration. The optical response is modeled using transfer matrix method (TMM), where a plane wave of unit amplitude is incident from air onto the top DBR, while only a forward propagating transmitted wave is allowed at the substrate side, corresponding to open boundary conditions. A detailed description of the simulated VCSELs device cross-section used in MATLAB model is provided in (Chaqmaqchee, 2024). Due to their compact cavity volume and typically very short cavity length, VCSELs require DBR mirrors with very high reflectivity (~99%) to ensure proper laser operation with contrasting refractive indices (low and high). By precisely reflecting the light, these mirrors form a vertical resonator helping to maintain optical conditions for stable lasing operation (Shi, Wang, and Hu, 2009), with each layer having an optical thickness of one quarter of the operating wavelength (λ/4n) (Hestroffer et al., 2018). Achieving high reflectivity requires a greater contrast in refractive indices, which is a crucial factor in evaluating reflectivity. The reflectivity (R) of the DBRs structure can be calculated using the relation (Karim et al., 2000).

$$= \frac{\left(1 \quad qap \quad\right)}{\left(1 \quad qap \quad\right)} \left(1 - \frac{\alpha\lambda}{n \left(1 \quad p\right)}\right) \tag{1}$$

Where q, a, and p are the ratios of refractive indices, representing the incident, mirror, and exit mediums, respectively. λ is the centered wavelength, α is the effective absorption loss from the mirrors, and n_H is the high refractive index.

Following the DBRs, the active region of a VCSELs is composed QWs, which provides an optical gain in reflection mode. To provide effective optical enhancement, the vertical

resonator's standing wave on is located at the center antinode and achieves the standing wave condition $m\lambda/2n_c$ (Liu et al., 2019), where the mode number is m = 2. The design parameters are carefully chosen to support the formation of standing waves and promote optimal light emission at the desired wavelength, as presented in Table II. Specifically, the VCSEL was designed with four different N concentrations in the $GaNxAs_{1-x}$ QWs to investigate their influence on device performance.

Carefully optimizing the cavity length and DBR reflectivity for the target wavelength is essential for maximizing reflection gain and achieving high-efficiency lasing. The widely recognized Fabry-Perot reflection mode gain (G_r) calculations are (Vasileiadis et al., 2008).

$$G_r = \frac{\left(\sqrt{R_f} - \sqrt{R_b}g_s\right)^2 + 4\sqrt{R_f R_b}g_s sin^2\theta}{\left(1-\sqrt{R_f R_b}g_s\right)^2 + 4\sqrt{R_f R_b}g_s sin^2\theta} \quad (2)$$

where R_f and R_b are the reflectivity of the front and back mirrors, respectively. g_s is the single-pass gain, and Θ is the single-pass phase detuning. We can get the highest gain with minimum Θ.

In addition to internal losses, mirror loss caused by incomplete reflectivity of the top and bottom DBR mirrors plays a significant role in determining whether the threshold gain can be reached. This behavior is necessary due to the VCSEL rely on short cavity lengths, thus requiring DBRs with high reflectivity to achieve lasing. The mathematical expressions for the round-trip gain (g_s) and mirror loss (α_m) are indicated as (Kimura et al., 2003, Xie et al., 2015):

$$g_s = exp\left[\xi g L_a - \alpha_c L_c\right] \quad (3)$$

where ξ is gain enhancement factor, g is material gain, L_a is thickness of active region, α_c is cavity losses, and L_c is the effective cavity length.

$$\alpha_m = \frac{1}{L_c} In\left(\frac{1}{\sqrt{R_f R_b}}\right) \quad (4)$$

TABLE II
Designed VCSEL Layer Structure and Corresponding Layer Thicknesses for Different N Concentrations (x) in GaN_xAs_{1-x} QWs

Materials	Layer details	Thicknesses (nm)			
		x=0.4%	x=1.2%	x=2%	x=3%
AlAs	18-pairs top DBRs	80.65	89.3	95.8	101.1
GaAs		68.3	75.99	81.7	86.3
AlGaAs	Top-spacer	80	96.5	108.5	118
GaAs	5-QWs/7-Barriers	12	12	12	12
GaN_xAs_{1-x}		10	10	10	10
GaAs		12	12	12	12
AlGaAs	Bottom-spacer	80	96.5	108.5	118
GaAs	24-pairs bottom DBRs	68.3	75.99	81.7	86.3
AlAs		80.65	89.3	95.8	101.1
GaAs	Substrate				

AlAs; Aluminum arsenide, AlGaAs: Aluminum gallium arsenide, GaAs: Gallium arsenide, GaN_xAs_{1-x}: Gallium arsenide nitride, N: Nitrogen, QWs: Quantum wells, VCSELs: Vertical-cavity surface-emitting lasers, DBRs: Distributed Bragg reflectors

III. Results And Discussion

As previously stated, DBRs are key components of VCSELs (Hestroffer et al., 2018). We used two binary compounds (AlAs and GaAs), which are almost perfectly lattice-matched. As seen in Fig. 2a, the composition of Al and Ga varies. In AlAs/GaAs, we observe a high refractive index contrast between two materials, approximately around (Δn = 0.5), leading to maximal reflectivity in DBRs with reduced layers. AlAs/GaAs DBRs have many reflectivity spectra as seen in Fig. 2b. The DBRs for the various center (design) wavelengths of 954 nm, 1050 nm, 1122 nm, and 1181 nm are shown by each curve. These variations result from the AlAs and GaAs DBR layers' varying optical thicknesses. Reflection at the design wavelength is enhanced by constructive interference since each layer is usually a quarter-wavelength thick (λ/4n). The Bragg condition is altered when the layer thickness is changed. The reflectivity peak is shifted toward longer wavelengths when the optical thickness is increased. As illustrated below, the black curve with the thinner layers reflects at approximately 954 nm, whereas the green curve with the larger layers reflects at around 1181 nm. Beyond this range, the reflectivity quickly decreases. As shown in Fig. 2b, each reflectivity curve exhibits a broad, flat-top high reflectivity region, known as the stopband, where reflection reach its maximum. Fig. 2c illustrates that this stopband arises from the periodic structure of the DBR, which causes nearly fully reflected within this wavelength range, preventing transmission through the mirror. As the design wavelength increases, the stopband width significantly widens from 128 nm at 954 nm to 150 nm at 1181 nm. VCSELs operating at long wavelengths therefore benefit from the wider reflection band maintained by DBRs designed for these wavelengths, ensuring stable optical confinement and efficient lasing performance. Fig. 2d illustrates how the reflectivity spectrum varies when an optical cavity is formed between the DBRs by inserting an active area that contains GaN_xAs_{1-x} QWs. The QW area displays four distinct curves that represent the various N concentrations (x = 0.4%, 1.2%, 2%, and 3%). In GaN_xAs_{1-x}, increasing x (N content) results in a decrease in the active layer's band gap and an increase in the cavity's total optical thickness. As a result, longer wavelengths become the resonant wavelength. The optical cavity length between the mirrors in the cavity is an integer multiple of 1/2λ of the resonant modes. Strong optical field intensity is localized inside the cavity at these resonance frequencies. Cavity resonances, where light is absorbed rather than reflected, are shown as dips in the reflectivity curve. These locations correspond to potential VCSEL lasing wavelengths. The change in these dips with x indicates that the emission wavelength is tuned by the composition of the material to longer wavelength.

Fig. 3 displays the complete vertical structure of the VCSEL, comprising the top DBRs, cavity (active region and spacer layers), and bottom DBRs. The blue line represents the refractive index profile, while the red line shows the corresponding standing wave electric field intensity distribution. The optical field is strongly confined within the

http://dx.doi.org/10.14500/aro.12716

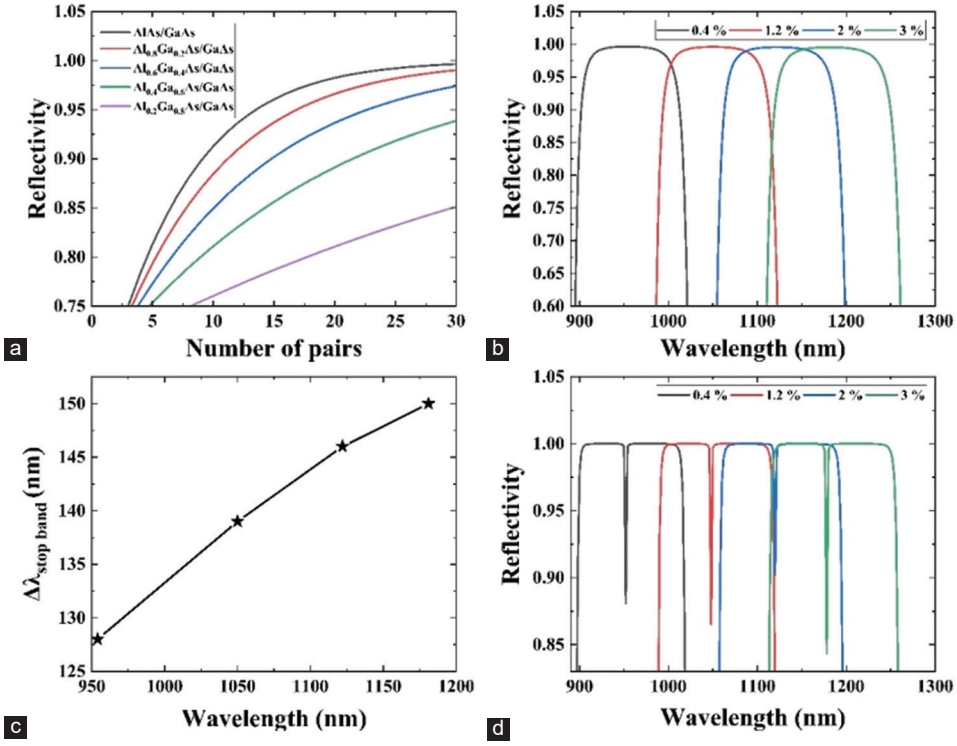

Fig. 2. Reflectivity characteristics of AlxGa1-xAs/GaAs-structures. (a) reflectivity as a function of the number of pairs for different Al compositions, (b) zoomed reflectivity of an 18-pairs of AlAs/GaAs DBR as a function of emitting wavelength, (c) stop band versus emitting wavelength, (d) zoomed reflectivity spectra for different N content of GaN_xAs_{1-x}/GaAs cavity with fixed 18-pairs of top DBRs and 24-pairs of bottom DBRs. GaAs: Gallium arsenide, AlxGa1-xAs: Aluminum gallium arsenide, AlAs: Aluminum arsenide, DBR: Distributed Bragg reflector, N: Nitrogen, GaN_xAs_{1-x}: Gallium arsenide nitride.

cavity area and gradually decays into DBR regions. The peak of electric field intensity is aligned with the QW for each N concentration. The standing wave maxima coincide with the QW, and the highest intensity is concentrated at the center of active region. This confirms that the cavity is completely resonant at the designed wavelength. A zoomed-in view of the QWs region, which consists of five GaNAs wells, reveals the concentration of electric field localization at the QWs, thereby maximizing optical confinement and improving efficiency of the VCSELs. Fig. 4 illustrates the effect of N concentration on mirror loss and threshold gain. In Fig. 4a, the mirror loss gradually decreases progressively as the N content in GaNAs increases. This reduction is attributed to changes in the optical properties of GaNAs with increasing N concentration. As additional N is incorporated, the emission wavelength of the VCSEL undergoes a redshift (shifts toward longer wavelengths), effectively increasing the optical cavity length. For a fixed mirror reflectivity, a longer effective cavity length leads to a reduced mirror loss. In Fig. 4b, the threshold modal gain (red curve) and internal loss (blue curve) both decrease as the N concentration increases up to around 2%, after which both parameters begin to rise again. The bandgap and photon energy are reduced when N atoms are added to the GaNAs material at low N concentrations (<2%). However, beyond ~2% N concentration, excessive N incorporation introduces alloy disorder, leading to localized defect states and composition fluctuations. These imperfections increase internal optical loss through enhanced scattering and non-radiative recombination. Consequently, a higher modal gain is required to overcome these additional losses, resulting in the observed increase in threshold gain for N concentration above 2%.

Dependence of key VCSEL parameters on N concentration x in GaN_xAs_{1-x} is shown in Fig. 5. Fig. 5a illustrates the variation of threshold carrier density (red curve) and carrier transparency (blue curve) with N concentration. Higher N concentration raises both values. Band tail states are created when N is introduced, which trap electrons and holes. Band flattening and a decrease in the conduction-band curvature result from the introduction of localized states by N that interact with the conduction band through the band anticrossing process. Specifically, increasing N concentration alters the conduction-band curvature through band-anticrossing interactions, which leads to changes in the electron effective mass and the density of states, as summarized in Table III. Since the transparency carrier density is strongly dependent on the carrier effective masses, these variations result in the observed shift in transparency density. The threshold carrier density exhibits a similar trend because it is governed by the transparency carrier density in conjunction with the internal and mirror losses of the optical cavity. The optical gain per carrier decreases, requiring more carriers to achieve population inversion. As a result, the threshold carrier density and the carrier transparency both rises. More injected carriers

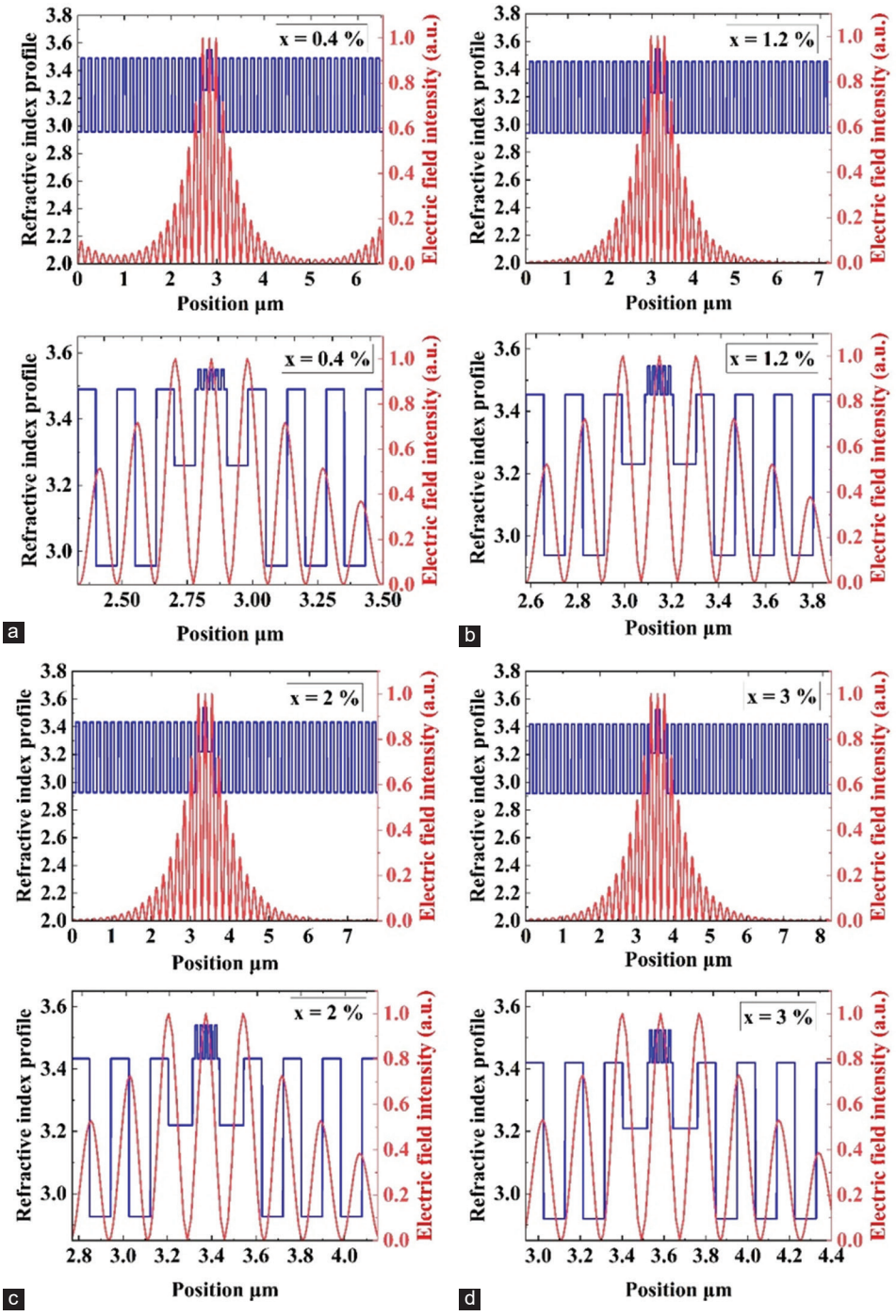

Fig. 3. Refractive index profile and standing optical wave pattern of the VCSEL structure for different N concentrations in GaN_xAs_{1-x}, (a) 0.4% N, (b) 1.2% N, (c) 2% N, and (d) 3% N. For each of (a-d), the lower panels show a zoomed- in view of s along with the corresponding optical intensity distribution. VCSEL: Vertical-cavity surface-emitting laser, N: Nitrogen, QWs: Quantum wells, GaN_xAs_{1-x}: Gallium arsenide nitride.

are required to attain the lasing threshold at greater N levels due to the further reduction in radiative recombination efficiency caused by increased non-radiative centers and carrier localization. Fig. 5b shows the variation of the optical confinement factor in GaN_xAs_{1-x} with concentration x. The confinement factor steadily drops from approximately 0.12–0.093 as the N percentage gets higher from 0.4% to 3%. A decreased overlap between the optical field and the gain medium results from the optical mode becoming less confined to the active area and more propagated into the spacer layers. This drop in confinement factor raises the carrier density needed to cross the lasing threshold. Table III presents the key parameters, including refractive indices, electron effective mass, hole effective mass, and band gap values. Fig. 6 presents the dependence of material gain and carrier density for different N ratios. In all cases, the material gain increases non-linearly with carrier density, demonstrating the saturation behavior of the gain mechanism. However, the gain

http://dx.doi.org/10.14500/aro.12716

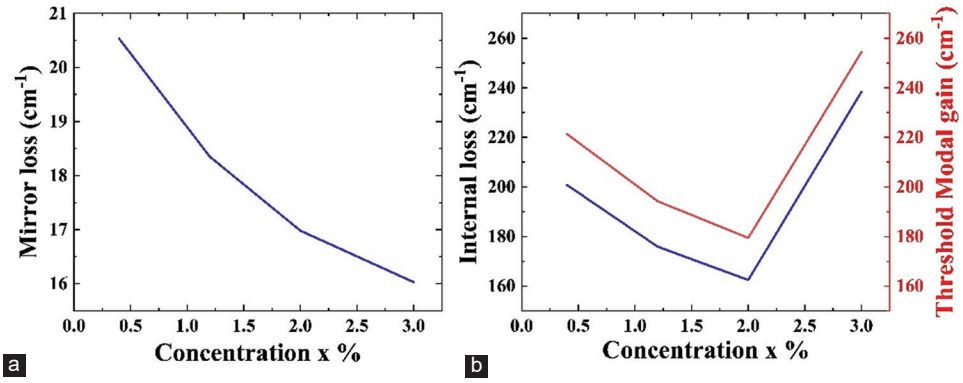

Fig. 4. Effect of N concentration x in GaN_xAs_{1-x} on (a) mirror loss and (b) internal loss and threshold modal gain. N: Nitrogen, GaN_xAs_{1-x}: Gallium arsenide nitride.

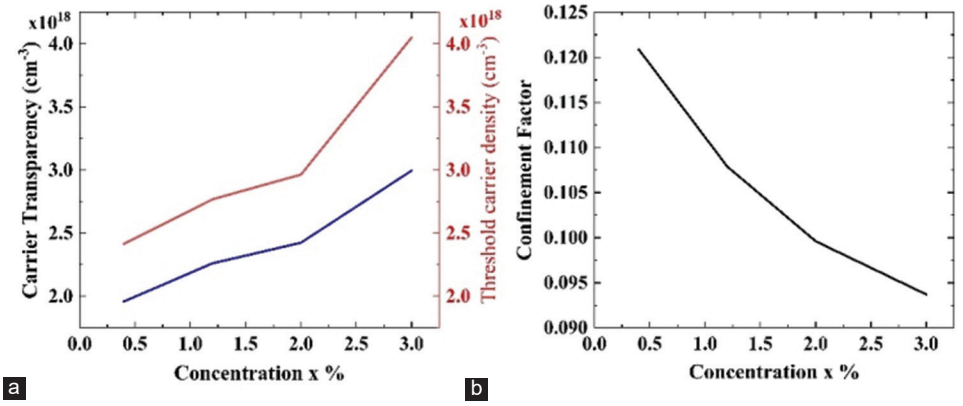

Fig. 5. Effect of N concentration x in GaN_xAs_{1-x} on carrier and optical properties, (a) carrier transparency and threshold carrier density, (b) optical confinement factor. N: Nitrogen, GaN_xAs_{1-x}: Gallium arsenide nitride.

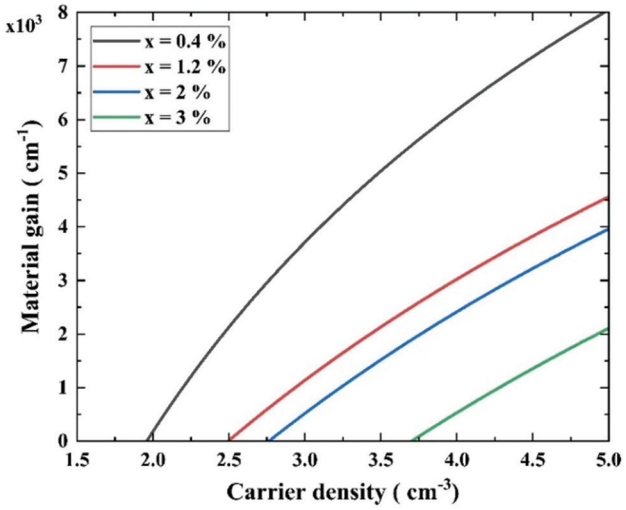

Fig. 6. Material gains of GaN_xAs_{1-x} for various N concentrations as a function of carrier density in the vertical cavity surface-emitting laser structure. N: Nitrogen, GaN_xAs_{1-x}: Gallium arsenide nitride.

curves shift downward with increasing N content, resulting in lower gain values at the same carrier density. This behavior is due to the reduction in the energy bandgap as the N content increases, which modifies the electronic band structure and lowers the optical transition probability. The carrier density at which the material transitions from absorbing light to amplifying it is called the carrier transparency density. Below N_t, the material absorbs photons rather than producing gain. Above N_t, the material generates net optical gain, enabling amplification and lasing.

Modal gain of the GaN_xAs_{1-x} based VCSEL cavity is shown in Fig. 7a-d for N concentrations of x = 0.4%, 1.2%, 2%, and 3%, respectively. The resonance peak in each spectrum exhibits a strong and distinct resonance peak, corresponding to the cavity mode that occurs when constructive interference develops between the two DBRs. At x = 0.4% (Fig. 7a), the emission wavelength at about 954 nm with a peak gain of around 24 dB. As the N increases to x = 3% (Fig. 7d), the resonance wavelength shifts to approximately 1181 nm, with the peak gain reduced to around 10 dB. This shift is due to the reduction in the band gap of GaN_xAs_{1-x}, which occurs as the N content increases. Furthermore, when the concentration of N increases, the strength of the peak gain steadily decreases. This decrease is attributed to the reduction in material gain caused by the bandgap narrowing, which decreases the optical transition probability. In addition, the reduction of the optical confinement factor allows more optical energy to leak into the spacer and DBR layers. As a result, the peak gain decreases with higher N concentrations, indicating a reduction in the overall amplification efficiency of the cavity, although a distinct resonance peak is still observed throughout all the N

TABLE III
CALCULATION PARAMETERS FOR DIFFERENT N CONCENTRATION IN GaN_xAs_{1-x} VCSEL

Parameters	Nitrogen concentration				References
	x=0.4%	x=1.2%	x=2%	x=3%	
AlAs refractive index (n_{AlAs})	2.957	2.938	2.927	2.92	(Fern and Onton, 1971)
GaAs refractive index (n_{GaAs})	3.49	3.454	3.433	3.42	(Skauli et al., 2003)
QWs refractive index (n_{QW})	3.55	3.545	3.54	3.525	(Leibiger et al., 2001)
Spacer refractive index (n_{spacer})	3.26	3.23	3.22	3.21	(Adachi, 1985)
Cavity refractive index (n_c)	3.37	3.33	3.31	3.29	
Effective cavity length (L_c)	2.9370 µm	3.2861 µm	3.5511 µm	3.7613 µm	
QWs (GaNAs) band gap (Eg)	1.3 eV	1.18 eV	1.105 eV	1.05 eV	(Takeuchi et al., 1998)
Electron effective mass of GaNAs (m_e)	0.085 m_o	0.103 m_o	0.113 m_o	0.15 m_o	(Ryczko et al., 2013)
Heavy hole effective mass of GaNAs (m_{hh})	0.37 m_o	0.37 m_o	0.37 m_o	0.37 m_o	(Gladysiewicz et al., 2013)
Light hole effective mass of GaNAs (m_{lh})	0.0804 m_o	0.08 m_o	0.08 m_o	0.079 m_o	(Gladysiewicz et al., 2013)
Carrier transparency (N_t)	1.958×10^{18} cm^{-3}	2.261×10^{18} cm^{-3}	2.424×10^{18} cm^{-3}	2.995×10^{18} cm^{-3}	
Threshold carrier density (N_{th})	2.41×10^{18} cm^{-3}	2.769×10^{18} cm^{-3}	2.964×10^{18} cm^{-3}	4.05×10^{18} cm^{-3}	

AlAs: Aluminum arsenide, VCSELs: Vertical-cavity surface-emitting lasers, QWs: Quantum wells, GaNAs: Gallium nitride arsenide, GaN_xAs_{1-x}: Gallium arsenide nitride, N: Nitrogen

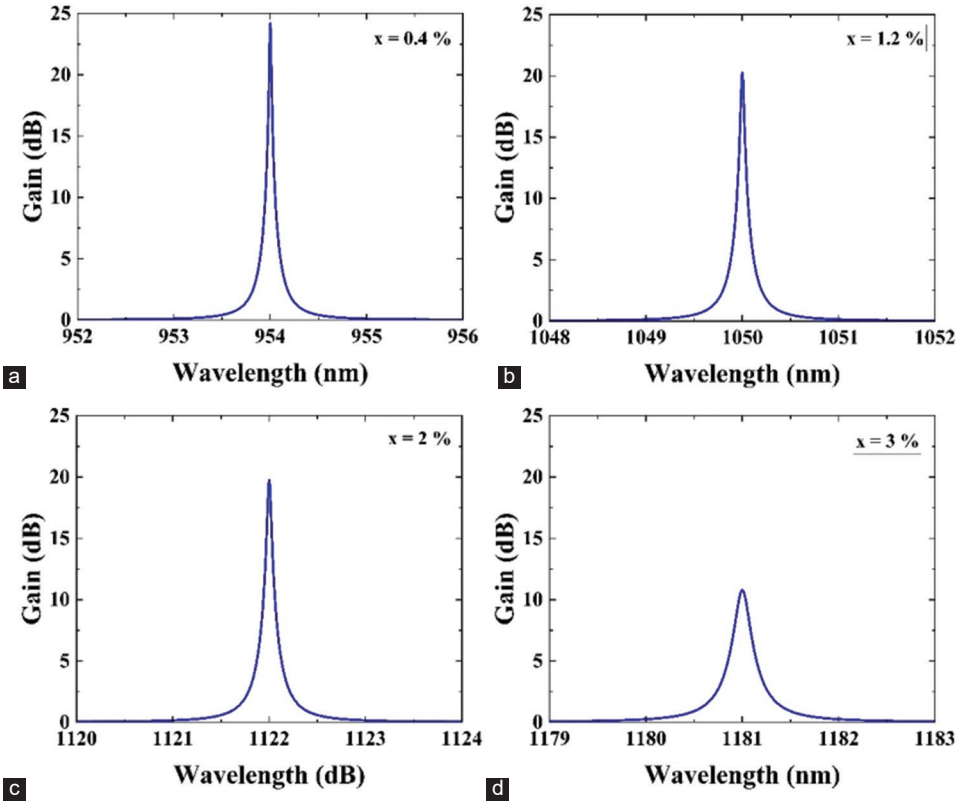

Fig. 7. (a-d) The reflection-mode gain spectra versus wavelength for GaN_xAs_{1-x} in reflection mode with varying concentration x. GaN_xAs_{1-x}: Gallium arsenide nitride.

concentrations. Fig. 8 presents the variation of optical gain (blue line), and Q-factor (red line) as a function of N concentrations in GaN_xAs_{1-x} ranging from 0.4% to 3%. Both the optical gain and the Q-factor decrease progressively as the N content increases. At a low N concentration of approximately 0.4%, the maximum gain reaches about 24 dB, and the Q-factor is at its highest. When the N concentration increases to 3%, both parameters decrease significantly, with the gain dropping to roughly 10 dB and the Q-factor reaching its minimum value. This decline indicates weakened optical feedback, resulting in a decreased cavity gain. Higher N concentrations increase interface roughness and scattering losses, which lower the cavity's Q-factor, a parameter that characterizes the resonator's ability to confine optical radiation. Therefore, the reduction in both gain and Q-factor at elevated N concentration clearly reflects the overall cavity optical performance in GaN_xAs_{1-x}.

IV. CONCLUSION

This work evaluated the impact of different N concentrations on device performance by analyzing the optical and gain properties of GaN_xAs_{1-x} based VCSELs using MATLAB simulations. Due to the optical path varies as the N concentration increases, the reflectivity spectra

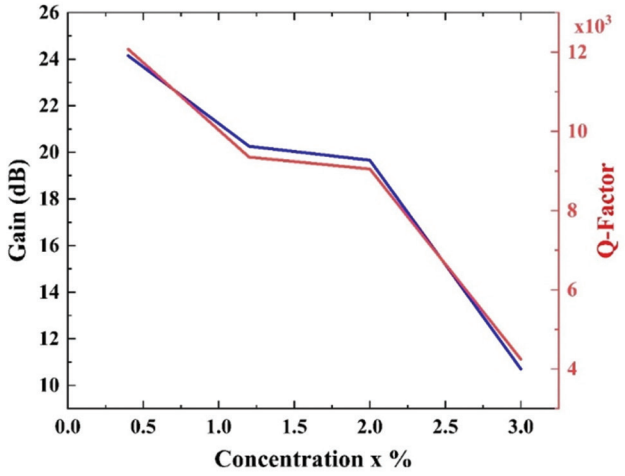

Fig. 8. Variation of optical gain and Q-factor as a function of N concentration in GaN_xAs_{1-x}. N: Nitrogen, GaN_xAs_{1-x}: Gallium arsenide nitride.

indicated that the resonance wavelength goes broader toward the longer wavelength. The standing-wave pattern and peak regions inside the QWs shifted in parallel with the rising N concentration, reflecting this shift in the spatial distribution of the electric field strength. In addition, the results demonstrated that as the percentage of N increased, mirror loss decreased, which is improved reflectivity. Indicating a trade-off between optical confinement and scattering losses, the internal loss and threshold modal gain showed a non-linear variation, first declining, and afterwards increasing above 2% of N. Furthermore, increasing the N fraction leads to a reduction in the overlap between the optical mode the active region, which consequently decreases both the optical confinement factor and the material gain. Higher N incorporation also increases the threshold carrier density and the carrier transparency, indicating reduced carrier confinement efficiency. The reflection-mode spectra confirm a redshift in the lasing wavelength with increasing N concentration, accompanied by a decrease in the gain peak intensity. Overall, for the GaN_xAs_{1-x} QWs based VCSEL, the optimal of optical performance and gain efficiency is achieved at using N concentration of approximately 1–2%. The confinement factor, the losses, and the gains of these specific N concentrations are (0.11, 0.099), (175 cm^{-1}, 162 cm^{-1}), and (20.26 dB, 19.66 dB), respectively.

V. Acknowledgments

This work was conducted as part of the PhD program of the department of Physics (DPHY), Faculty of Science and Health, Koya University, in the Kurdistan region of Iraq. The author sincerely thanks the supervisors for their valuable advice and continuous support through this research.

References

Abdullah, A.I., and Chaqmaqchee, F.A.I., 2025. Design and simulation of 850 nm InGaAs QWs vertical cavity surface emitting lasers for enhanced optical interconnects. *Journal of Optics*. Doi: https://doi.org/10.1007/s12596-025-02903-4

Adachi, S., 1985. GaAs, AlAs, and $Al_xGa_{1-x}As$: Material parameters for use in research and device applications. *Journal of Applied Physics*, 58, pp.R1-R29.

Alexandre, F., Gouardes, E., Gauthier-Lafaye, O., Bouadma, N., Vuong, A., and Thedrez, B., 2002. Nitride-based long-wavelength lasers on GaAs substrates. *Journal of Materials Science Materials in Electronics*, 13, pp.633-642.

Babichev, A.V., Pirogov, E.V., Sobolev, M.S., Denisov, D.V., Fominykh, H.A., Baranov, A.I., Gudovskikh, A.S., Melnichenko, I.A., Yunin, P.A., Nevedomsky, V.N., Tokarev, M.V., Ber, B.Y., Gladyshev, A.G., Karachinsky, L.Y., Novikov, I.I., and Egorov, A.Y., 2023. Study of active regions based on multiperiod GaAsN/InAs superlattice. *Semiconductors*, 57, pp.474-482.

Balakrishnan, N., Pettinari, G., Makarovsky, O., Hopkinson, M., and Patanè, A., 2014. Tunable spectral response by hydrogen irradiation of Ga(AsN) superlattice diodes. *Applied Physics Letters*, 104, p.242110.

Buyanova, I.A., Chen, W.M., Pozina, G., Hai, P.N., Monemar, B., Xin, H.P., and TU, C.W., 2001. Optical properties of GaNAs/GaAs structures. *Materials Science and Engineering B*, 82, pp.143-147.

Cao, Y., 2020. Development of vertical cavity surface emitting laser modulation for data communication. *Journal of Physics Conference Series*, 1653, p.012001.

Chakir, K., Bilel, C., Habchi, M.M., Rebey, A., and El Jani, B., 2017. Theoretical study of the carrier effective mass in diluted III-N-V semiconductor alloys by using 10-band k.p model. *Thin Solid Films,* 630, pp.25-30.

Chaqmaqchee, F.A., 2016. Optical design of dilute nitride quantum wells vertical cavity semiconductor optical amplifiers for communication systems. *Aro The Scientific Journal of Koya University*, 4, pp.8-12.

Chaqmaqchee, F.A., 2020. Long-wavelength GaInNAs/GaAs vertical-cavity surface-emitting laser for communication applications. *ARO the Scientific Journal of Koya University*, 8, pp.107-111.

Chaqmaqchee, F.A.I., 2024. Fabrication and characterization of stable temperature and reliable size oxide aperture VCSELs for short-reach communication. *Journal of Optics*, 53, pp.3453-3462.

Chaqmaqchee, F.A.I., Salh, S.A.A., Faeq, M., Sabri, M.M.J.Z.J.O.P., and Sciences, A., 2020. Optical analysis of 1300 nm GaInNAsSb/GaAs vertical cavity semiconductor optical amplifier. *ZANCO Journal of Pure and Applied Sciences*, 32, pp.87-92.

Ebeling, K.J., Michalzik, R., and Moench, H., 2018. Vertical-cavity surface-emitting laser technology applications with focus on sensors and three-dimensional imaging. *Japanese Journal of Applied Physics*, 57, p.08PA02.

Fern, R.E., and Onton, A., 1971. Refractive index of AlAs. *Journal of Applied Physics,* 42, pp.3499-3500.

Fujii, K., Takao, K., Kumamoto, T., Kakino, M., Tsurumachi, N., Miyagawa, H., Ueji, R., Itoh, H., Nakanishi, S., Akiyama, H., and Koshiba, S., 2007. GaNAs/GaAs multiple quantum well grown by modulated N radical beam sequence of RF-MBE: Effect of growth interruption. *Journal of Crystal Growth*, 301-302, pp.583-587.

Gelczuk, Ł., Dąbrowska-szata, M., Ściana, B., Pucicki, D., Radziewicz, D., Kopalko, K., and Tłaczała, M., 2016. Characterization of deep-level defects in GaNAs/GaAs heterostructures grown by APMOVPE. *Materials Science Poland*, 34, pp.726-734.

Gilli, L., Cossu, G., and Ciaramella, E., 2025. New prospects of optical wireless communication systems exploiting VCSEL-Based Transmitters. *Journal of Lightwave Technology*, 43, pp.1615-1624.

Gladysiewicz, M., Kudrawiec, R., MIloszewski, J.M., Weetman, P., Misiewicz, J., and Wartak, M.S., 2013. Band structure and the optical gain of GaInNAs/GaAs quantum wells modeled within 10-band and 8-band kp model. *Journal of Applied Physics,* 113, p.063514.

Goshima, K., Kittaka, A., Fujii, K., Shiraga, M., Tsurumachi, N., Nakanishi, S., Akiyama, H., Koshiba, S., and Itoh, H., 2011. Investigation of the confinement

potential within GaNAs/GaAs multiple quantum wells. *Physica Status Solidi C*, 8, pp.414-416.

Guina, M., Wang, S.M., and Aho, A., 2018. Molecular beam epitaxy of dilute nitride optoelectronic devices. In: Henini, M., Eds. *Molecular Beam Epitaxy (Second Edition).* Ch. 5. Elsevier, Sweden.

Hai, P.N., Chen, W.M., Buyanova, I.A., Xin, H.P., and Tu, C.W., 2000. Direct determination of electron effective mass in GaNAs/GaAs quantum wells. *Applied Physics Letters*, 77, pp.1843-1845.

Hestroffer, K., Sperlich, D., Dadgostar, S., Golz, C., Krumland, J., Masselink, W.T., and Hatami, F., 2018. Transport properties of doped AlP for the development of conductive AlP/GaP distributed Bragg reflectors and their integration into light-emitting diodes. *Applied Physics Letters*, 112, p.192107.

Jaffal, A., Boulay, P., Vallo, M., and Dogmus, E., 2024. *VCSELs Market Outlook in Consumer Sensing and Data Communication. In: Proceedings Volume 12904, Vertical-Cavity Surface-Emitting Lasers XXVIII, 2024*. SPIE, United States, pp.58-62.

Jansson, M., Nosenko, V.V., Torigoe, Y., Nakama, K., Yukimune, M., Higo, A., Ishikawa, F., Chen, W.M., and Buyanova, I.A., 2024. High-performance multiwavelength GaNAs single nanowire lasers. *ACS Nano*, 18, pp.1477-1484.

Karim, A., Bjorlin, S., Piprek, J., and Bowers, J.E., 2000. Long-wavelength vertical-cavity lasers and amplifiers. *IEEE Journal of Selected Topics in Quantum Electronics*, 6, pp.1244-1253.

Kimura, T., Bjorlin, S., Piprek, J., and Bowers, J.E., 2003. High-temperature characteristics and tunability of long-wavelength vertical-cavity semiconductor optical amplifiers. *IEEE Photonics Technology Letters*, 15, pp.1501-1503.

Leibiger, G., Gottschalch, V., Rheinländer, B., Šik, J., and Schubert, M., 2001. Model dielectric function spectra of GaAsN for far-infrared and near-infrared to ultraviolet wavelengths. *Journal of Applied Physics*, 89, pp.4927-4938.

Li, H., Wolf, P., Moser, P., Larisch, G., Lott, J.A., and Bimberg, D.J., 2015. Temperature-stable, energy-efficient, and high-bit rate oxide-confined 980-nm VCSELs for optical interconnects. *IEEE Journal of Selected Topics in Quantum Electronics*, 21, pp.405-413.

Lisesivdin, S.B., Khan, N.A., Mazzucato, S., Balkan, N., Adams, M.J., Korpijärvi, V.M., Guina, M., Mezosi, G., and Sorel, M., 2014. Optical gain in 1.3-μm electrically driven dilute nitride VCSOAs. *Nanoscale Research Letters*, 9, p.22.

Liu, A., Wolf, P., Lott, J.A., and Bimberg, D., 2019. Vertical-cavity surface-emitting lasers for data communication and sensing. *Photonics Research*, 7, pp.121-136.

Moatlhodi, O.O., Ditshego, N.M., and Samikannu, R.J., 2020. Vertical cavity surface emitting lasers as sources for optical communication systems: A review. *Journal of Nano Research*, 65, pp.51-96.

Muszalski, J., Sankowska, I., and Kucharski, S., 2020. Nanoindentation of GaAs/AlAs distributed bragg reflector grown on GaAs substrate. *Materials Science in Semiconductor Processing*, 109, p.104912.

Onishi, Y., Saga, N., Koyama, K., Doi, H., Ishizuka, T., Yamada, T., Fujii, K., Mori, H., Hashimoto, J. I., Simazu, M., Yamaguchi, A., and Katsuyama, T., 2009. Long-wavelength GalnNAs VCSEL with buried tunnel junction current confinement structure. *IEEE Journal of Selected Topics in Quantum Electronics*, 15, pp.40-43.

Pozina, G., Ivanov, I., Monemar, B., Thordson, J., and Andersson, T.J., 1998. Optical properties of GaNAs grown by MBE. *Journal of Nitride Semiconductor Research*, 3, p.e29.

Ryczko, K., Sęk, G., Sitarek, P., Mika, A., Misiewicz, J., Langer, F., Höfling, S., Forchel, A., and Kamp, M., 2013. Verification of band offsets and electron effective masses in GaAsN/GaAs quantum wells: Spectroscopic experiment versus 10-band k·p modeling. *Journal of Applied Physics*, 113, p.233508.

Sanna, S., and Fiorentini, V., 2004. Lattice constant, effective mass, and gap recovery in hydrogenated $GaAs_{1-x}N_x$. *Physical Review B*, 69, p.125208.

Shi, X., Qi, C., Wang, G., and Hu, J., 2009. *Rate-Equation-Based VCSEL Model and Simulation. In: 2009 11th IEEE International Conference on Computer-Aided Design and Computer Graphics*. IEEE, United States, pp.503-507.

Skauli, T., Kuo, P.S., Vodopyanov, K.L., Pinguet, T.J., Levi, O., Eyres, L.A., Harris, J.S., Fejer, M.M., Gerard, B., Becouarn, L., and Lallier, E., 2003. Improved dispersion relations for GaAs and applications to nonlinear optics. *Journal of Applied Physics,* 94, pp.6447-6455.

Sun, Y., Cheng, Z., Zhou, Q., Sun, Y., Sun, J., Liu, Y., Wang, M., Cao, Z., Ye, Z., Xu, M., Ding, Y., Chen, P., Heuken, M., and Egawa, T., 2018. Redshift and blueshift of GaNAs/GaAs multiple quantum wells induced by rapid thermal annealing. *Journal of Crystal Growth,* 483, pp.190-194.

Swara, J.A., Chaqmaqchee, F.A., and Sediq, K.N., 2025. High reflectivity compounds of cadmium sulfide/magnesium fluoride distribution bragg reflectors: Design, simulation, and comparative analysis. *Aro The Scientific Journal Of Koya University,* 13, pp.160-166.

Takao, K., Fujii, K., Miyagawa, H., Mizumaki, M., Sakata, O., Tsurumachi, N., Itoh, H., Sumida, N., Nakanishi, S., Akiyama, H., and Koshiba, S., 2006. Growth of GaNAs/GaAs multiple quantum well by molecular beam epitaxy using modulated N radical beam source. *Japanese Journal of Applied Physics*, 45, p.3540.

Takeuchi, K., Miyamoto, T., Kageyama, T., Koyama, F., and Iga, K., 1998. Chemical beam epitaxy growth and characterization of GaNAs/GaAs. *Japanese Journal of Applied Physics*, 37, p.1603.

Tian, S.C., Ahamed, M., and Bimberg, D., 2023. Progress in short wavelength energy-efficient high-speed vertical-cavity surface-emitting lasers for data communication. *Photonics*, 10, p.410.

Vasileiadis, M., Alexandropoulos, D., Adams, M.J., Simos, H., and Syvridis, D.J., 2008. Potential of InGaAs/GaAs quantum dots for applications in vertical cavity semiconductor optical amplifiers. *IEEE Journal of Selected Topics in Quantum Electronics,* 14, pp.1180-1187.

Wang, J., Cui, N., Wang, H., Shi, Z., Zhang, F., Fu, L., and Guan, B., 2025. Heterogeneous integration, single-mode MEMS-VCSEL with super-span resonance filtering, small divergence angle, and Gaussian distribution. *Optics Express,* 33, pp.15316-15326.

Watanabe, T., Yokozeki, M., Takanohashi, M., Shiomi, M., Nakajima, H., Tanaka, M., Kasahara, D., Kobayashi, N., and Futagawa, N., 2025. 1380 nm VCSELs using surface-activated bonding of GaAs-based DBRs on a Ge substrate. *Applied Physics Express,* 18, p.016507.

Wu, C.K., Xue, X.E., Tian, S.C., Miah, M.J., Strittmatter, A., and Bimberg, D., 2024. Improvement of beam quality of high-power edge-emitting lasers using inhomogeneous waveguides. *Optics Express,* 32, pp.24802-24810.

Xie, Y., Xu, C., Kan, Q., Xun, M., Xu, K., and Chen, H., 2015. Polarization stable low threshold current single fundamental mode VCSELs. *Optical Materials Express,* 5, pp.1998-2005.

Xu, K., Cheng, D., and Huang, X., 2009. *Multimode Communication System used in Local Area Network (LAN). In: 2009 Symposium on Photonics and Optoelectronics*, IEEE, United States, pp.1-4.

Yaba, H.I., and Chaqmaqchee, F.A., 2022. Design, modeling, and characterization of hot electron light emission and lasing in semiconductor heterostructure-VCSOA with optical gain up to 36 dB. *Aro-the Scientific Journal of Koya University,* 10, pp.111-115.

Yu, T.C., Huang, W.T., Wang, H.C., Chiu, A.P., Kou, C.H., Hong, K.B., Chang, S.W., Chow, C.W., and Kuo, H.C.J.M., 2023. Design and simulation of InGaN-based red vertical-cavity surface-emitting lasers. *Micromachines (Basel)*, 15, p.87.

Zhang, Z., Von Würtemberg, R.M., Berggren, J., and Hammar, M., 2007. Optical loss and interface morphology in AlGaAs/GaAs distributed Bragg reflectors. *Applied Physics Letters*, 91, p.101101.